Supporting Information

Investigation of Freezing-Induced Anionic Interplay in Acoustically Levitated Artificial Seawater Droplets

Frank Liang[a], Souvick Biswas[a], Nils W Melbourne[a], Koushik Mondal[a], Rui Sun[a], Ralf Kaiser[a]*

[a] Department of Chemistry, University of Hawai'i at Manoa, Honolulu, Hawaii 96822, United States

* Corresponding authors. E-mail: ralfk@hawaii.edu

Contents:

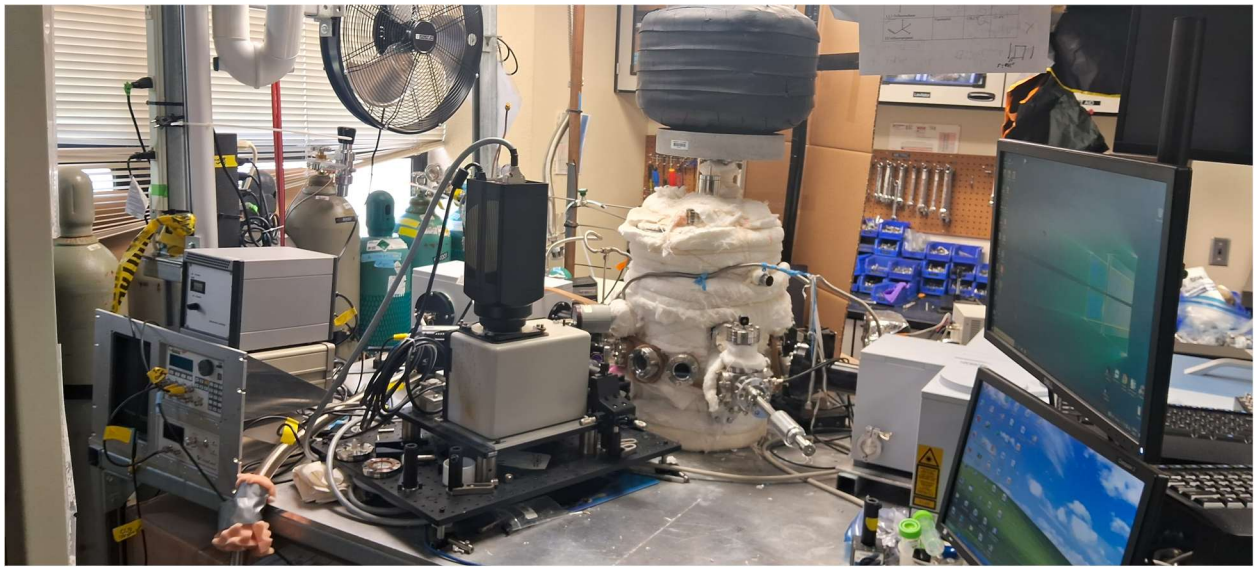

Figure S1: Photograph of the levitator setup.

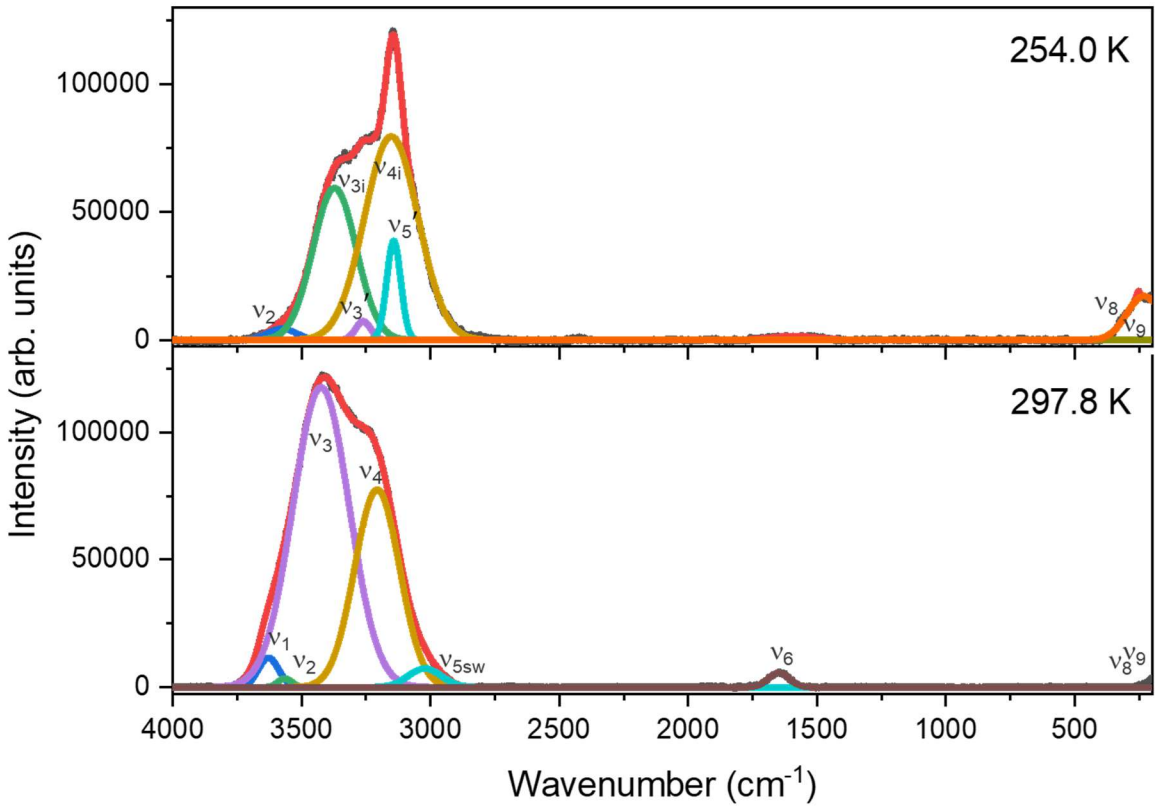

Figure S2: Deconvoluted Raman spectra of pure water droplet in its liquid form at 297.8 K, and when it is frozen at 254.0 K.

Table S1: Peak assignments for the deconvoluted Raman spectrum of the ice crystal made of pure water at 254.0 K.

Peak	Experimental wavenumber (cm^{-1})	Carrier	Peak assignment	Literature wavenumber (cm^{-1})	Reference
ν_2	3577	H_2O (surface)	O-H stretch (weakly or non H-bonded OH)	~3600	[1-3]
ν_{3i}	3372	H_2O (bulk)	O-H stretch (red-shifted intermediate H-bond)	3314	[2, 4-6]
ν_3'	3262	H_2O (bulk)	Symmetric OH stretch	3270	[6]
ν_{4i}	3153	H_2O (deformed)	Red-shifted O-H stretch of deformed tetrahedral H-bond	~3200	[1-2]
ν_5'	3143	H_2O (bulk)	O-H stretch of strong H-bond or ion stabilized water	3140	[2, 6-8]
ν_6	1589	H_2O	OH bend	~1600	[9-10]
ν_8	255	SO_4^{2-} (aq)	Translational lattice mode	~280	[7, 11]
ν_9	232	H_2O (bulk)	Translational lattice mode	~220	[7, 11]

Table S2: Peak assignments for the deconvoluted Raman spectrum of the pure water droplet at 297.8 K.

Peak	Experimental wavenumber (cm^{-1})	Carrier	Peak assignment	Literature wavenumber (cm^{-1})	Reference
ν_1	3631	H_2O (surface)	O-H stretch (free, non H-bonded OH)	~3600	[1]
ν_2	3564	H_2O (surface)	O-H stretch (weakly H-bonded OH)	~3530	[12]
ν_3	3425	H_2O (bulk)	Bulk water O-H intermediate stretch	3435	[12-13]
ν_4	3208	H_2O (deformed)	O-H stretch of deformed tetrahedral H-bond	3140- ~3200	[1-2, 6-7]
ν_{5sw}	3019	H_2O (bulk)	Intense O-H stretching	~2800-3000	[14-15]
ν_6	1608	H_2O	OH bend	~1600	[9-10]
ν_8	255	SO_4^{2-} (aq)	Translational lattice mode	~280	[7, 11]
ν_9	232	H_2O (bulk)	Translational lattice mode	~280	[7, 11]

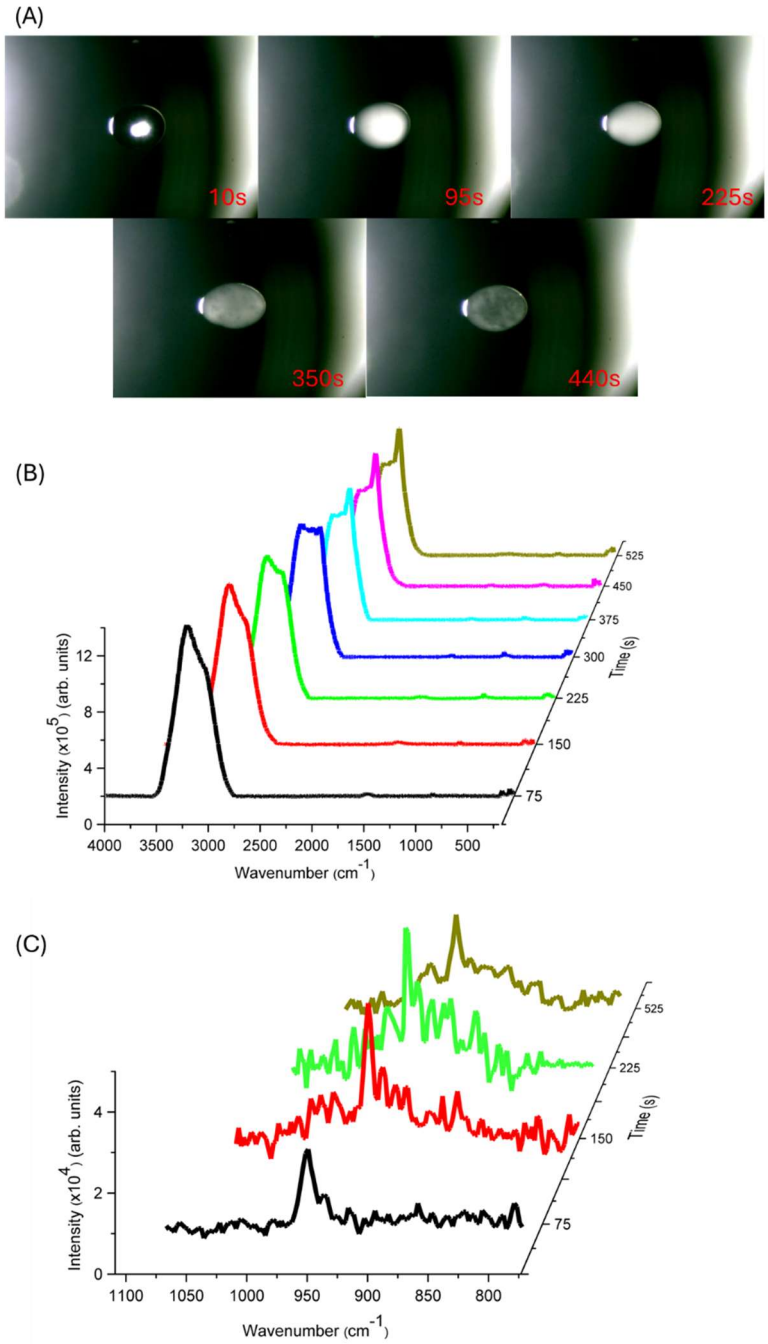

Figure S3: (A) Visualization of the freezing process of the levitating seawater droplet with time. (B) The time-dependent Raman spectra showing the change in the physical state and molecular structure evolution of seawater droplet during freezing. The broad spectral region ~3800-2800 cm^{-1} is the O-H stretching frequencies arising out of different kinds of intermolecular interactions. (C) Zoomed in time-dependent spectra of the droplet/ice particle at selected times at the 1100-800 cm^{-1} region where changes related to the sulfate peak are observed.

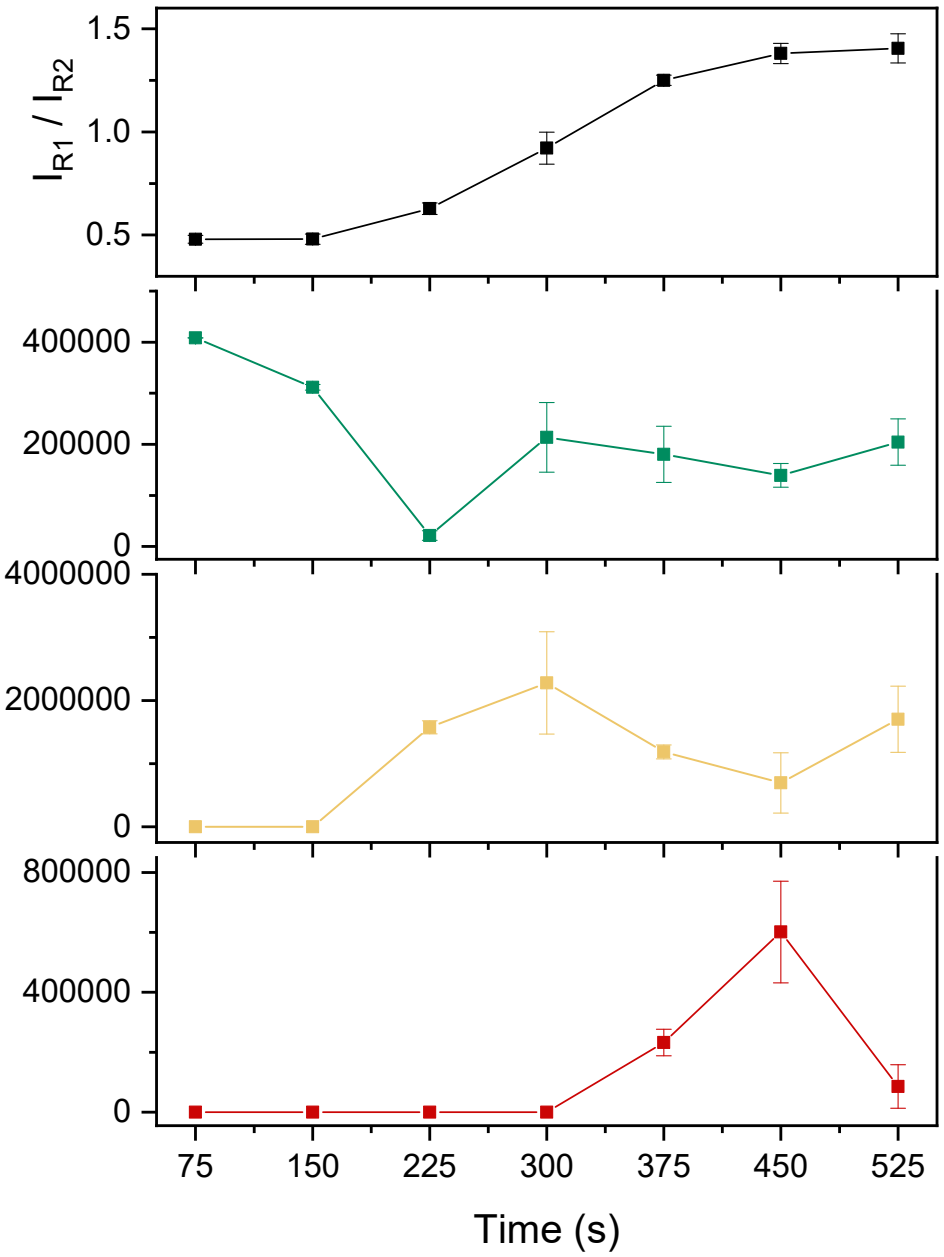

Figure S4. (A) Temporal profile of the water/ice features during the aqueous droplet freezing process. The freezing process is quantified by evaluating the ratios of corresponding areas of two spectral segments from 3200 to 3100 cm^{-1} and 3440 to 3340 cm^{-1}, which correspond to specific features of ice and liquid water, respectively. (B) Temporal profile of the sulfate stretching peak located at around 981 cm^{-1}. (C) Temporal profile of the distorted sulfate stretch peak located at 916-951 cm^{-1}. (D) Temporal profile of the bisulfate stretch peak located at around 1013 cm^{-1}.

Table S3: Peak assignments for the deconvoluted Raman spectrum of the aqueous droplet containing 3.5% $MgSO_4$ solution at 297.8 K as shown in Figure 3(A).

Peak	Experimental wavenumber (cm^{-1})	Carrier	Peak assignment	Literature wavenumber (cm^{-1})	Reference
ν_1	3641	H_2O (surface)	O-H stretch (non-H-bonded)	3632	[1-3]
ν_2	3583	H_2O (surface)	O-H stretch (weakly or non H-bonded OH)	~3600	[1-3]
ν_3	3426	H_2O (bulk)	Intermediate OH stretch	3314-3435	[12-13]
ν_4	3224	H_2O (bulk)	O-H stretch of deformed tetrahedral H-bond	3140- ~3200	[1-2, 6-7]
ν_5	3105	H_2O (bulk)	O-H stretch of ideal tetrahedral H-bond	3075	[1]
ν_6	1637	H_2O (bulk)	OH bend	~1600	[9-10]
ν_{7s}	1014	HSO_4^- (aq)	S-O stretch in bisulfate	1050	[16]
ν_7	981	SO_4^{2-} (aq)	Symmetric S-O stretch in sulfate	981	[17]
ν_{8s}	614	SO_4^{2-} (aq)	ν_4 bending of sulfate	613	[18]
ν_{9s}	446	SO_4^{2-} (aq)	ν_2 bending of sulfate	451	[18]
ν_8	260	H_2O (l)	Translational lattice mode	~280	[7, 11]
ν_9	225	H_2O (l)	Translational lattice mode	~220	[7, 11]

s = sulfate solution being the first time this mode appears.

Table S4: Peak assignments for the deconvoluted Raman spectrum of the aqueous ice crystal containing 3.5% $MgSO_4$ solution at 254.0 K as shown in Figure 3(B).

Peak	Experimental wavenumber (cm^{-1})	Carrier	Peak assignment	Literature wavenumber (cm^{-1})	Reference
ν_{1s}'	3566	H_2O (surface)	O-H stretch of fully coordinated interfacial water molecules	~3530	[12]
ν_{3i}	3370	H_2O (bulk)	Bulk water O-H stretch (red-shifted intermediate H-bond)	3314-3435	[2, 4-6, 12-13]
ν_{2s}'	3252	H_2O (deformed)	O-H stretch of hexagonal crystal structure	3208	[5]
ν_{4i}	3152	H_2O (s)	O-H stretch of deformed tetrahedral H- bond	3140- ~3200	[1-2, 6-7]
ν_5'	3137	H_2O (s)	O-H stretch in DDAA ice	3140-3150	[2, 6-7]
ν_{5sw}	2878	H_2O (bulk)	Intense O-H stretching	~2800-3000	[14-15]
ν_6	1625	H_2O (bulk)	OH bend	~1600	[9-10]
ν_7'	1014	SO_4^{2-} (aq/s)	Symmetric S-O stretch of sulfate in reduced symmetry environments	1000	[19]
ν_7	980	SO_4^{2-} (aq)	Symmetric S-O stretch in sulfate	981	[17]
ν_8'	916	SO_4^{2-} (aq/s)	Symmetric S-O stretch of sulfate in reduced symmetry environments		[18, 20-21]
ν_{8s}	602	SO_4^{2-} (aq)	ν_4 bending of sulfate	613	[18]
ν_{9s}	452	SO_4^{2-} (aq)	ν_2 bending of sulfate	451	[18]
ν_8	280	H_2O (s)	Translational lattice mode	~280	[7, 11]
ν_9	227	H_2O (s)	Translational lattice mode	~220	[7, 11]

Table S5: Peak assignments for the deconvoluted Raman spectrum of the aqueous droplet containing 3.5% $NaHCO_3$ solution at 297.8 K as shown in Figure 4(A).

Peak	Experimental wavenumber (cm^{-1})	Carrier	Peak assignment	Literature wavenumber (cm^{-1})	Reference
ν_1	3636	H_2O (surface)	O-H stretch (free, non H-bonded OH)	~3600	[1]
ν_2	3579	H_2O (surface)	O-H stretch (weakly H-bonded OH)	~3530	[12]
ν_3	3417	H_2O (bulk)	Intermediate OH stretch	3435	[12-13]
ν_4	3221	H_2O (bulk)	O-H stretch of deformed tetrahedral H-bond	3140- ~3200	[1-2, 6-7]
ν_5	3106	H_2O (bulk)	O-H stretch of ideal tetrahedral H-bond	3075	[1]
ν_{5b}*	2620	HCO_3^- (aq)	CO-H stretch	2619	[22]
ν_6	1627	H_2O (bulk)	O-H bend	1630	[9-10, 23]
ν_{7b}	1370	HCO_3^- (aq)	CO_2 stretch	1360	[22, 24]
ν_{8b}	1309	HCO_3^- (aq)	C-OH bend	1302	[22, 24-25]
ν_{9b}	1014	HCO_3^- (aq)	C-OH stretch	1014	[22, 25-26]
ν_{10b}	676	HCO_3^- (aq)	CO_2 bending	673	[22, 24]
ν_{11b}	642	HCO_3^- (aq)	OCO or HOC deformation	641	[22, 24]
ν_8	281	H_2O (l)	Translational lattice mode	~280	[7, 11]
ν_9	222	H_2O (l)	Translational lattice mode	~220	[7, 11]

b = bicarbonate solution being the first time this mode appears.

Table S6: Peak assignments for the deconvoluted Raman spectrum of the aqueous ice crystal containing 3.5% $NaHCO_3$ solution at 254.0 K as shown in Figure 4(B).

Peak	Experimental wavenumber (cm^{-1})	Carrier	Peak assignment	Literature wavenumber (cm^{-1})	Reference
ν_{1s}'	3574	H_2O (surface)	O-H stretch of fully coordinated interfacial water molecules	~3530	[12]
ν_{3i}	3369	H_2O (bulk)	O-H stretch (intermediate H-bond)	3314-3435	[2, 4-6, 12-13]
ν_{2s}'	3253	H_2O (deformed)	O-H stretch of hexagonal crystal structure	3208	[5]
ν_{4i}	3153	H_2O (s)	O-H stretch of deformed tetrahedral H-bond	3140- ~3200	[1-2, 6-7]
ν_5'	3138	H_2O (s)	O-H stretch in DDAA* ice	3140-3150	[2, 6-7]
ν_{5b}	2622	HCO_3^- (aq)	CO-H stretch	2619	[22]
ν_6	1628	H_2O (bulk)	OH bend	~1600	[9-10]
ν_{7b}	1374	HCO_3^- (aq)	CO_2 stretch	1364	[22, 26]
ν_{8b}	1309	HCO_3^- (aq)	C-OH bend	1300-1312	[22, 25-26]
ν_{9b}	1018	HCO_3^- (aq)	C-OH stretch	1016	[22, 25-26]
ν_{10b}	682	HCO_3^- (aq)	CO_2 bending	673	[22]
ν_{11b}	647	HCO_3^- (aq)	OCO or HOC deformation	641	[22]
ν_8	293	H_2O (s)	Translational lattice mode	~280	[7, 11]
ν_9	239	H_2O (s)	Translational lattice mode	~220	[7, 11]

Table S7: Peak assignments for the deconvoluted Raman spectrum of the aqueous droplet containing 3.5% $MgSO_4$ and $NaHCO_3$ 1:1 mass ratio solution at 297.8 K as shown in Figure 5(A).

Peak	Experimental wavenumber (cm^{-1})	Carrier	Peak assignment	Literature wavenumber (cm^{-1})	Reference
ν_1	3637	H_2O (surface)	O-H stretch (free, non H-bonded OH)	~3600	[1]
ν_2	3583	H_2O (surface)	O-H stretch (weakly H-bonded OH)	~3530	[12]
ν_3	3417	H_2O (bulk)	Intermediate OH stretch	3435	[12-13]
ν_4	3226	H_2O (bulk)	O-H stretch of deformed tetrahedral H- bond	3140- ~3200	[1-2, 6-7]
ν_5'	3130	H_2O (s)	O-H stretch in DDAA ice	3140-3150	[2, 6-7]
ν_{5b}	2620	HCO_3^- (aq)	CO-H stretch	2619	[22]
ν_6	1628	H_2O (bulk)	OH bend	~1600	[9-10]
ν_{6m}	1458	CO_3^{2-} (aq)	Asymmetrical stretching of C-O from CO_3^{2-}	1400-1450	[24, 27-28]
ν_{7b}	1361	HCO_3^- (aq)	CO_2 stretch	1364	[22, 26]
ν_{8b}	1318	HCO_3^- (aq)	C-OH bend	1300-1312	[22, 25-26]
ν_{9b}	1013	HCO_3^- (aq)	C-OH stretch	1016	[22, 25-26]
ν_7	978	SO_4^{2-} (aq)	Symmetric S-O stretch in sulfate	981	[17]
ν_{10b}	681	HCO_3^- (aq)	CO_2 bending	673	[22, 24]
ν_{11b}	650	HCO_3^- (aq)	OCO or HOC deformation	641	[22, 24]
ν_{8s}	604	SO_4^{2-} (aq)	v4 bending of sulfate	613	[18]
ν_{9s}	454	SO_4^{2-} (aq)	v2 bending of sulfate	451	[18]
ν_8	295	H_2O (l)	Translational lattice mode	~280	[7, 11]
ν_9	234	H_2O (l)	Translational lattice mode	~220	[7, 11]

m = mixture solution of bicarbonate and sulfate being the first time this mode appears.

Table S8: Peak assignments for the deconvoluted Raman spectrum of the aqueous ice crystal containing 3.5% $MgSO_4$ and $NaHCO_3$ 1:1 mass ratio solution at 254.0 K as shown in Figure 5(B).

Peak	Experimental wavenumber (cm^{-1})	Carrier	Peak assignment	Literature wavenumber (cm^{-1})	Reference
ν_{1s}'	3577	H_2O (surface)	O-H stretch (weakly H-bonded OH)	~3530	[12]
ν_{3i}	3384	H_2O (bulk)	O-H stretch (intermediate H-bond)	3314-3435	[2, 4-6, 12-13]
ν_{2s}'	3248	H_2O (deformed)	O-H stretch of hexagonal crystal structure	3208	[5]
ν_{4i}	3160	H_2O (s)	O-H stretch of strong H-bond)	3140- ~3200	[1-2, 6-7]
ν_5'	3139	H_2O (s)	O-H stretch in DDAA ice	3140-3150	[2, 6-7]
ν_{5b}	2610	HCO_3^- (aq)	CO-H stretch	2619	[22]
ν_6	1616	H_2O (bulk)	OH bend	~1600	[9-10]
ν_{6m}	1453	CO_3^{2-} (aq)	Asymmetrical stretching of C-O from CO_3^{2-}	1400-1450	[24, 27-28]
ν_{7b}	1362	HCO_3^- (aq)	CO_2 stretch	1364	[22, 26]
ν_{8b}	1318	HCO_3^- (aq)	C-OH bend	1300-1312	[22, 25-26]
ν_{9b}	1012	HCO_3^- (aq)	C-OH stretch	1016	[22, 25-26]
ν_7	977	SO_4^{2-} (aq)	Symmetric S-O stretch in sulfate	981	[17]
ν_8'	943	SO_4^{2-} (aq/l)	Symmetric S-O stretch of sulfate in reduced symmetry environments		[18, 20-21]
ν_{11b}	638	HCO_3^- (aq)	OCO or HOC deformation	641	[22, 24]
ν_{9s}	466	SO_4^{2-} (aq)	v2 bending of sulfate	456	[17-18]
ν_8	290	H_2O (s)	Translational lattice mode	~280	[7, 11]
ν_9	239	H_2O (s)	Translational lattice mode	~220	[7, 11]

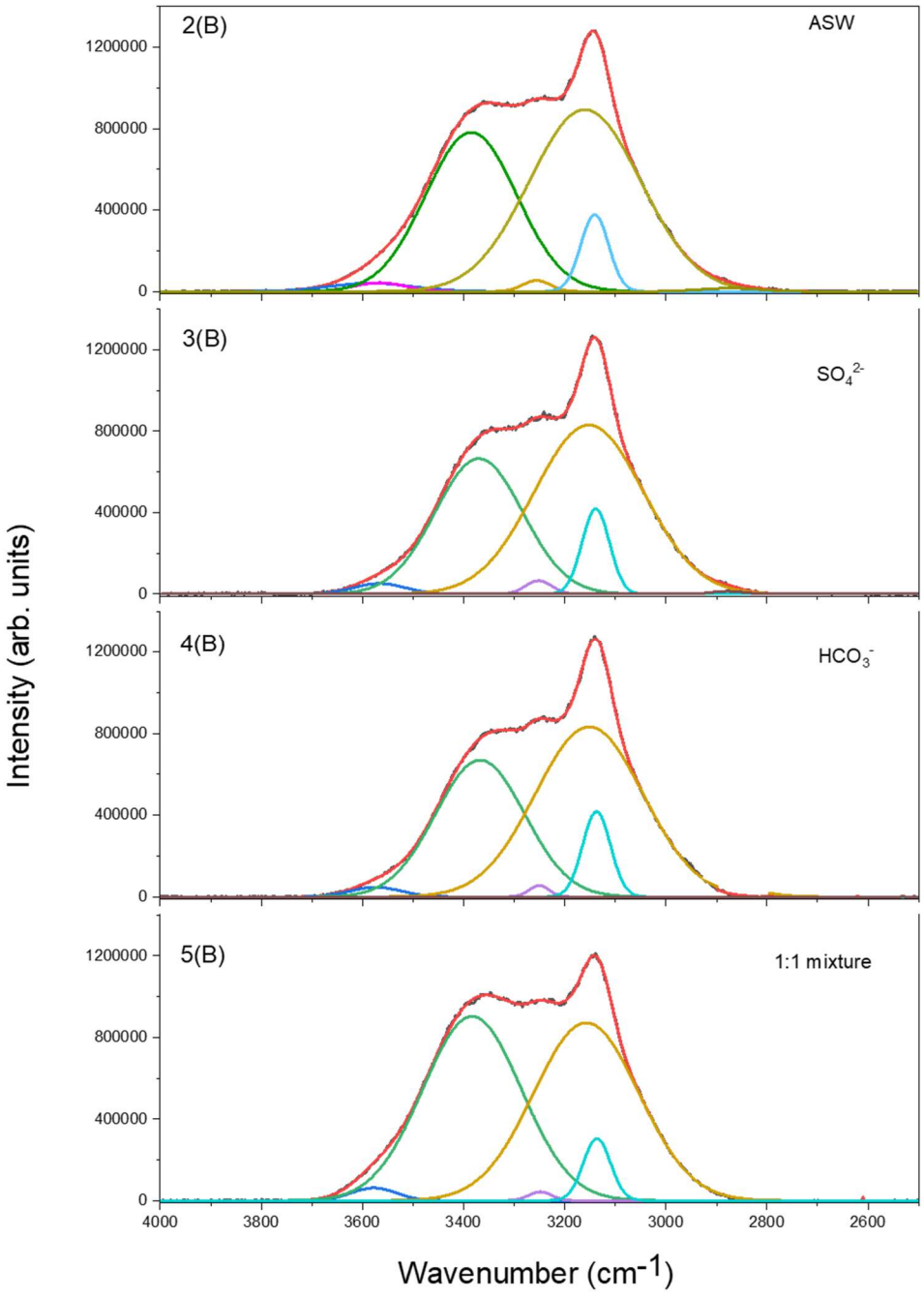

Figure S5: Stacked spectra from Figures 2(B), 3(B), 4(B) and 5(B), showing the comparisons of deconvoluted bands of the OH-stretching region of the ice crystals at 254.0 K.

Table S9: Full width at half-maximum (FWHM) for the fitted bands of the deconvoluted OH-region of the ice crystal of ASW at 254.0 K.

Peak	Experimental wavenumber (cm^{-1})	Peak width (cm^{-1})
ν_1	3583	100
ν_{1s}'	3566	121
ν_{3i}	3380	212
ν_{2s}'	3256	64
ν_{4i}	3160	259
ν_5'	3140	65
ν_{5sw}	2874	138

Table S10: Full width at half-maximum (FWHM) for the fitted bands of the deconvoluted OH-region of the ice crystal containing $MgSO_4$ solution at 254.0 K.

Peak	Experimental wavenumber (cm^{-1})	Peak width (cm^{-1})
ν_{1s}'	3566	120
ν_{3i}	3370	204
ν_{2s}'	3252	61
ν_{4i}	3152	254
ν_5'	3137	64
ν_{5sw}	2878	73

Table S11: Full width at half-maximum (FWHM) for the fitted bands of the deconvoluted OH-region of the ice crystal containing HCO_3 solution at 254.0 K.

Peak	Experimental wavenumber (cm^{-1})	Peak width (cm^{-1})
ν_{1s}'	3574	118
ν_{3i}	3369	208
ν_{2s}'	3253	47
ν_{4i}	3153	251
ν_5'	3138	65

Table S12: Full width at half-maximum (FWHM) for the fitted bands of the deconvoluted OH-region of the ice crystal containing 1:1 mixture of $MgSO_4$ and HCO_3 solution at 254.0 K.

Peak	Experimental wavenumber (cm^{-1})	Peak width (cm^{-1})
ν_{1s}'	3577	102
ν_{3i}	3384	222
ν_{2s}'	3248	48
ν_{4i}	3160	235
ν_{5}'	3139	89

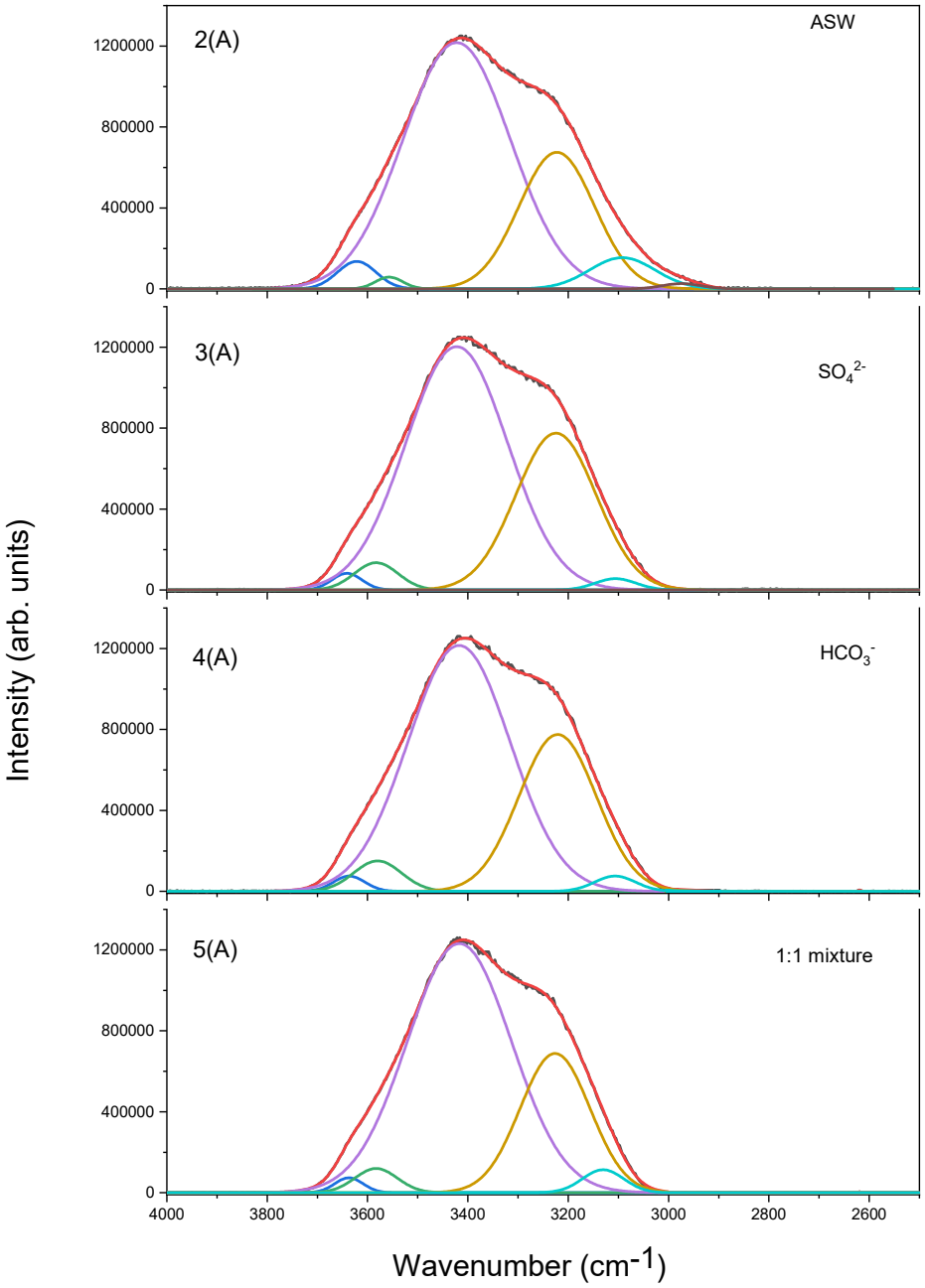

Figure S6: Stacked spectra from Figures 2(A), 3(A), 4(A) and 5(A), showing the comparisons of deconvoluted bands of the OH-stretching region of the droplets at 297.8 K.

Table S13: Full width at half-maximum (FWHM) for the fitted bands of the deconvoluted OH-region of the ASW droplet at 297.8 K.

Peak	Experimental wavenumber (cm^{-1})	Peak width (cm^{-1})
ν_1	3622	91
ν_2	3557	64
ν_3	3425	252
ν_4	3223	177
ν_5	3095	153
ν_{5SW}	2974	91

Table S14: Full width at half-maximum (FWHM) for the fitted bands of the deconvoluted OH-region of the $MgSO_4$ droplet at 297.8 K.

Peak	Experimental wavenumber (cm^{-1})	Peak width (cm^{-1})
ν_1	3641	71
ν_2	3583	102
ν_3	3426	238
ν_4	3224	189
ν_5	3105	96

Table S15: Full width at half-maximum (FWHM) for the fitted bands of the deconvoluted OH-region of the HCO_3 droplet at 297.8 K.

Peak	Experimental wavenumber (cm^{-1})	Peak width (cm^{-1})
ν_1	3636	74
ν_2	3579	112
ν_3	3417	240
ν_4	3221	182
ν_5	3106	96

Table S16: Full width at half-maximum (FWHM) for the fitted bands of the deconvoluted OH-region of the 1:1 mixture of $MgSO_4$ and HCO_3 droplet at 297.8 K.

Peak	Experimental wavenumber (cm^{-1})	Peak width (cm^{-1})
ν_1	3637	66
ν_2	3583	100
ν_3	3417	245
ν_4	3226	164
ν_5'	3130	97

References

1. Dong, C.; Liu, Y.; Han, T.; Zhou, X.; Meng, Y.; Tian, Y.; Ma, L., Effect of hydrated ions and wettability on ice friction. *Friction* **2025,** *13* (7), 1.
2. Sun, Q.; Zheng, H., Raman OH stretching vibration of ice Ih. *Prog. Nat. Sci.* **2009,** *19* (11), 1651-1654.
3. Wernet, P.; Nordlund, D.; Bergmann, U.; Cavalleri, M.; Odelius, M.; Ogasawara, H.; Naslund, L. A.; Hirsch, T.; Ojamae, L.; Glatzel, P., The structure of the first coordination shell in liquid water. *Science* **2004,** *304* (5673), 995-999.
4. Bergren, M. S.; Schuh, D.; Sceats, M. G.; Rice, S. A., The OH stretching region infrared spectra of low density amorphous solid water and polycrystalline ice Ih. *J. Chem. Phys.* **1978,** *69* (8), 3477-3482.
5. Furić, K.; Volovšek, V., Water ice at low temperatures and pressures: New Raman results. *J. Mol. Struct.* **2010,** *976* (1-3), 174-180.
6. Garcia, C. S.; Abedin, M. N.; Sharma, S. K.; Misra, A. K.; Ismail, S.; Singh, U. N.; Refaat, T. F.; Elsayed-Ali, H. E.; Sandford, S. P. In *Remote pulsed laser Raman spectroscopy system for detecting water, ice, and hydrous minerals*, Imaging Spectrometry XI, SPIE: 2006; pp 296-302.
7. Fukazawa, H.; Mae, S.; Ikeda, S., Raman scattering and neutron-diffraction studies of fresh ice and Antarctic ice. *Ann. Glaciol.* **2000,** *31*, 247-251.
8. Wall, T. T.; Hornig, D. F., Raman spectra of water in concentrated ionic solutions. *J. Chem. Phys.* **1967,** *47* (2), 784-792.
9. Shigenari, T.; Abe, K., Vibrational modes of hydrogens in the proton ordered phase XI of ice: Raman spectra above 400 cm− 1. *J. Chem. Phys.* **2012,** *136* (17).
10. Wong, P.; Whalley, E., Optical spectra of orientationally disordered crystal. V. Raman spectrum of ice Ih in the range 4000-350 cm-1. *J. Chem. Phys.* **1975,** *62* (6), 2418-2425.
11. Biswas, S.; Paul, D.; Mondal, K.; Kaiser, R. I., Simulating atmospheric freezing of single aqueous droplets to ice in a cryogenically cooled ultrasonic levitator. *Proc. Natl. Acad. Sci.* **2025,** *122* (6), e2425543122.
12. Smit, W. J.; Tang, F.; Nagata, Y.; Sánchez, M. A.; Hasegawa, T.; Backus, E. H.; Bonn, M.; Bakker, H. J., Observation and identification of a new OH stretch vibrational band at the surface of ice. *J. Phys. Chem. Lett.* **2017,** *8* (15), 3656-3660.
13. Walrafen, G., Raman and infrared spectral investigations of water structure. In *Phys. and Physical Chem. of Water*, Springer: 1972; pp 151-214.
14. Wang, Z.; Pakoulev, A.; Pang, Y.; Dlott, D. D., Vibrational substructure in the OH stretching transition of water and HOD. *The Journal of Physical Chemistry A* **2004,** *108* (42), 9054-9063.
15. Baumgartner, M.; Bakker, R. J., Raman spectroscopy of pure H2O and NaCl-H2O containing synthetic fluid inclusions in quartz—a study of polarization effects. *Mineralogy and Petrology* **2009,** *95* (1), 1-15.
16. Xi, S.; Zhang, X.; Luan, Z.; Du, Z.; Li, L.; Wang, B.; Cao, L.; Lian, C.; Yan, J., A direct quantitative Raman method for the measurement of dissolved bisulfate in acid-Sulfate fluids. *Appl. Spectrosc.* **2018,** *72* (8), 1234-1243.
17. Mabrouk, B.; Kauffmann, K.; Thomas H Aroui, H.; Fontana, M. D., Raman study of cation effect on sulfate vibration modes in solid state and in aqueous solutions. *J. Raman Spectrosc.* **2013,** *44* (11), 1603-1608.

18. Frost, R. L.; Xi, Y.; Scholz, R.; López, A.; Granja, A., Infrared and Raman spectroscopic characterisation of the sulphate mineral creedite–Ca3Al2SO4 (F, OH)· 2H2O–and in comparison with the alums. *Spectrochim. Acta - Part A Mol. Biomol. Spectrosc.* **2013,** *109*, 201-205.
19. Tran, L. K.; Stepien, K. R.; Bollmeyer, M. M.; Yoder, C. H., Substitution of sulfate in apatite. *Am. Mineral.* **2017,** *102* (10), 1971-1976.
20. Periasamy, A.; Muruganand, S.; Palaniswamy, M., Vibrational studies of Na2SO4, K2SO4, NaHSO4 and KHSO4 crystals. *Rasayan J. Chem* **2009,** *2* (4), 981-989.
21. Tuschel, D., Stress, strain, and Raman spectroscopy. **2019**.
22. Rudolph, W. W.; Irmer, G.; Königsberger, E., Speciation studies in aqueous HCO 3−–CO 3 2− solutions. A combined Raman spectroscopic and thermodynamic study. *J. Chem. Soc. Dalt. Trans.* **2008,** (7), 900-908.
23. Frezzotti, M. L.; Tecce, F.; Casagli, A., Raman spectroscopy for fluid inclusion analysis. *J. Geo. Explo.* **2012,** *112*, 1-20.
24. Frantz, J. D., Raman spectra of potassium carbonate and bicarbonate aqueous fluids at elevated temperatures and pressures: comparison with theoretical simulations. *Chem. Geol.* **1998,** *152* (3-4), 211-225.
25. Falcke, H.; Eberle, S., Raman spectroscopic identification of carbonic acid. *Water Res.* **1990,** *24* (6), 685-688.
26. Swartzwelder, A. D. Raman spectroscopy of the CO_2-H_2O system. The Ohio State University, 2006.
27. Alves, J. F.; Edwards, H. G.; Korsakov, A.; De Oliveira, L. F. C., Revisiting the Raman spectra of carbonate minerals. *Minerals* **2023,** *13* (11), 1358.
28. Bissengaliyeva, M., Calculations of the structural and thermodynamic characteristics of copper carbonates by quantum-chemical methods. *Russ. J. Phys. Chem. A* **2009,** *83* (2), 238-244.